Acta Biomaterialia 70 (2018) 57–70

Contents lists available at ScienceDirect

Acta Biomaterialia

journal homepage: www.elsevier.com/locate/actabiomat

Full length article

Cell reprogramming by 3D bioprinting of human fibroblasts in polyurethane hydrogel for fabrication of neural-like constructs

Lin Ho [a], Shan-hui Hsu [a,b,c,*]

[a] Institute of Polymer Science and Engineering, National Taiwan University, Taipei, Taiwan, ROC
[b] Center of Tissue Engineering and 3D Printing, National Taiwan University, Taipei, Taiwan, ROC
[c] Institute of Cellular and System Medicine, National Health Research Institutes, Zhunan, Taiwan, ROC

ARTICLE INFO

Article history:
Received 5 December 2017
Received in revised form 26 January 2018
Accepted 29 January 2018
Available online 7 February 2018

Keywords:
3D bioprinting
Cell reprogramming
Polyurethane
Shear stress
Neural tissue engineering

ABSTRACT

3D bioprinting is a technique which enables the direct printing of biodegradable materials with cells into 3D tissue. So far there is no cell reprogramming *in situ* performed with the 3D bioprinting process. Forkhead box D3 (FoxD3) is a transcription factor and neural crest marker, which was reported to reprogram human fibroblasts into neural crest stem-like cells. In this study, we synthesized a new biodegradable thermo-responsive waterborne polyurethane (PU) gel as a bioink. FoxD3 plasmids and human fibroblasts were co-extruded with the PU hydrogel through the syringe needle tip for cell reprogramming. The rheological properties of the PU hydrogel including the modulus, gelation time, and shear thinning were optimized for the transfection effect of FoxD3 *in situ*. The corresponding shear rate and shear stress were examined. Results showed that human fibroblasts could be reprogrammed into neural crest stem-like cells with high cell viability during the extrusion process under an average shear stress ~190 Pa. We further translated the method to the extrusion-based 3D bioprinting, and demonstrated that human fibroblasts co-printed with FoxD3 in the thermo-responsive PU hydrogel could be reprogrammed and differentiated into a neural-tissue like construct at 14 days after induction. The neural-like tissue construct produced by 3D bioprinting from human fibroblasts may be applied to personalized drug screening or neuroregeneration.

Statement of Significance

There is no study so far on cell reprogramming *in situ* with 3D bioprinting. In this manuscript, a new thermoresponsive polyurethane bioink was developed and employed to deliver FoxD3 plasmid into human fibroblasts by the extrusion-based bioprinting. When the polyurethane gel was extruded through the syringe tip, the shear stress generated may have caused the transient membrane permeability for transfection. The shear stress was optimized for transfection *in situ* by 3D bioprinting. We demonstrated that human fibroblasts could be reprogrammed into neural crest-like stem cells by 3D bioprinting with the gel, and the reprogrammed cells underwent neural differentiation in the printed structure after induction. The neural-like tissue engineering constructs fabricated by 3D bioprinting from human fibroblasts may be applied for neuroregeneration or further developed as mini-brain for basic research and drug screening.

© 2018 Acta Materialia Inc. Published by Elsevier Ltd. All rights reserved.

1. Introduction

Many adult neurological disorders such as stroke, Alzheimer disease, Parkinson's disease, and Huntington's disease still have no effective treatment today. Strategies designed to repair neurological diseases have been developed based on the neurogenerative capacities of the adult central neural system. Among them, cell therapies have the potential in treating these diseases [1,2]. Challenges remains because of the difficulty in expanding large numbers of neural stem cells in culture.

Induced pluripotent stem cells (iPSCs) were established in 2007. Human fibroblasts were first reprogrammed *in vitro* into iPSCs by the retroviral transduction of Oct4, Sox2, Klf4, and c-Myc genes

* Corresponding author at: Institute of Polymer Science and Engineering, National Taiwan University, No. 1, Sec. 4 Roosevelt Road, Taipei 10617, Taiwan, ROC.
E-mail address: shhsu@ntu.edu.tw (S.-h. Hsu).

https://doi.org/10.1016/j.actbio.2018.01.044
1742-7061/© 2018 Acta Materialia Inc. Published by Elsevier Ltd. All rights reserved.

in vitro [3], confirming that the somatic cells can be induced and reverted to be pluripotent, i.e., have the ability to differentiate into any cell types. This technology is considered to be a potential cell source for transplantation therapies, especially in neurodevelopmental and neurodegenerative diseases [4]. The iPSCs could be induced and differentiate into neural stem cells *in vitro* [5,6], which solves the demand for a large number of neural stem cells in therapies. With the recent development, somatic cells are directly reprogrammed into an alternate lineage without dedifferentiation into a pluripotent state [7]. The human fibroblasts could be directly reprogrammed into neural crest associated cells with Forkhead box D3 (FoxD3) gene delivered by a substrate mediated method [8]. This method provides a safer and more convenient approach to personalized cell transplantation therapies.

The process of gene transfection is necessary for generation of iPSCs and other types of induced cells. Gene transfection requires the exogenous gene to penetrate the cell membrane, while the membrane is impermeable to most external substances in order to protect cells. Transfection by viral vectors is the more effective gene delivery approach [9,10], but there are often risks of cytopathic effects from virus action. In addition to viral vectors, there are various non-viral methods to facilitate gene transfection, such as the use of transfection reagents, polymeric nanoparticles [11,12], liposomes [13], or physical methods [14–18], but all of which suffer from cell death and the cell-type dependent efficacy. A recent method based on rapid mechanical deformation of the cells by microfluidics to produce transient membrane disruptions to deliver genes has been developed [19,20]. "Squeezing cells" thus provides another strategy for cytosolic delivery.

Three-dimensional (3D) bioprinting has gained recent attention in the biomedical field. Among different bioprinting platforms, the extrusion-based bioprinting involves the extrusion of cells with supporting materials to build a tissue-like structure. Non-toxicity, biodegradability, and proper mechanical properties are essential requirements for the supporting materials of bioprinting. Although the shear stress during extrusion could injure the cells, it may also exert a transient mechanical force on the cell membrane. Here in this study, a new biodegradable thermo-responsive waterborne polyurethane (PU) gel was synthesized. The high water content and cytocompatibility allowed the embedded cells to survive. Moreover, the elasticity of the hydrogel may produce a "squeezing" effect on cells during extrusion. We tried to reprogram human fibroblasts *in situ* during the gelation and extruding process, where cells were embedded in the PU hydrogel with the FoxD3 plasmid, and extruded through the syringe needle of a 3D bioprinter. The printed cell-laden hydrogel may grow into a neural-tissue like construct. We expected to evaluate the feasibility of combining the cell reprogramming procedure with 3D bioprinting to produce customized tissue constructs.

2. Materials and methods

2.1. Synthesis of waterborne biodegradable PU1500

The PCL diol (M_n 2000 Da, Sigma-Aldrich) and poly(D,L-lactide) (PDLLA) diol (M_n ~1500 Da) were used as the soft segment to synthesize the new type of PU used in this study, which was abbreviated as PU1500. The PDLLA diol was synthesized from a ring-opening polymerization of lactide. The ring-opening agents, 1,3-propandiol (Alfa Aesar) and the catalyst T-9, were used to open the ring structure of D,L-lactide (Purac) at 145 °C for 8 h, and then purified by the absolute ethanol. The end-group analysis was using to confirm the molecular weight of oligodiol by nuclear magnetic resonance (NMR) spectroscopy. The previously reported type of PU was based on similar composition except that the PDLLA diol employed for synthesis had a different M_n (2000 Da), instead of 1500 Da. This former PU was used for comparison and abbreviated as PU2000. The PU dispersions were prepared as illustrated in Fig. S1. Both PUs (PU1500 and PU2000) contained 80% molar ratio of the PCL diol (M_n 2000 Da) and 20% molar ratio of the PDLLA diol (M_n 1500 or 2000 Da) in the soft segment. The detailed synthetic procedures were provided in earlier literature [21]. Briefly, The PCL diol and PDLLA diol were mixed under a nitrogen environment at 95 °C for 30 min, followed by addition of isophorone diisocyanate (IPDI, Evonik Degussa, GmbH). After the temperature was cooled to 75 °C, 2,2-bis(hydroxymethyl) propionic acid (DMPA, Sigma-Aldrich) and methyl ethyl ketone (MEK, J. T. Baker) were added. Triethylamine (TEA, RDH), ethylenediamine (EDA, Tedia), and deionized water were added under vigorous stirring to obtain water dispersion. The molar ratio of IPDI/oligodiols/DMPA/EDA/TEA was 3.52:1:1:1.52 : 1 [22]. The final water dispersion of PU was removed of the residual solvent and TEA. The aqueous dispersion contained ~30% PU and could be diluted to 25% in the cell culture medium.

2.2. Physico-chemical characterization

The PU dispersion for the experiments was diluted with deionized water or culture medium to a concentration of 2000 ppm. The components of culture medium [high glucose Dulbecco's Modified Eagle's Medium (HG-DMEM, Gibco, USA) with 1% sodium bicarbonate (Sigma-Aldrich, USA)] were added to the PU dispersion as the electrolytes. The concentration of the culture medium used to suspend PU was adjusted to the same concentration as that used for cell culture. The hydrodynamic diameter (D_h) of the PU dispersion in water or in culture medium was measured by dynamic light scattering (DLS; Delsa™ Nano Submicron particle analyzer, Beckman Coulter, USA), and the zeta potential was determined on the basis of electrophoretic light scattering measurements. The molecular weight of PU was determined by a JASCO gel permeation chromatography (GPC) system equipped with an refractive index detector (RI-930) using dimethylacetamide (DMAc) as the eluting solvent. ^{1}H- Nuclear magnetic resonance (^{1}H NMR; 400 MHz, Unity Inova FT-NMR, Varian, USA) spectra were obtained in $CDCl_3$. The morphology of PU1500 nanoparticles was examined by the transmission electron microscopy (TEM; JEM-1200EX II, JEOL, Japan) using 80 kV electron beam.

The Fourier transform infrared spectroscopy (FTIR, Spectrum 100 model, Perkin Elmer) with a setup of attenuated total reflection (ATR) mode was used to detect the abundance of hydrogen bond (H-bond) of PU films. The films were immersed into the culture medium for 24 h, rinsed and dried. Each film was scanned 16 times under a resolution of 1 cm^{-1} with the wavenumber range of 600 to –4000 cm^{-1}. The proportion of the hydrogen-bonded (H-bonded) C=O was obtained by the under-peak area of the H-bonded C=O at 1647 cm^{-1} divided by the sum of the under-peak area of the H-bonded C=O (1647 cm^{-1}) and that of the non-H-bonded C=O at 1730 cm^{-1}.

The thermogravimetric analysis (TGA; Perkin Elmer, TGA7, USA) was performed in 10 °C min^{-1} under N_2 to define the pyrolytic temperatures (T_{onset} at 50% weight loss and T_d at decomposition). The T_g and T_m were determined using a differential scanning calorimetry (DSC; Perkin Elmer, Pyris 6, USA) with a heating rate of 10 °C/min from −80 to 300 °C. The crystallization was determined by the DSC and an X-ray diffractometer (XRD; Bede D1, UK). The XRD data were obtained with a CuKα radiation (λ = 1.54 Å) source and the scan range of 2θ = 10° to –30°.

PU nanoparticles in aqueous media were analyzed by small-angle X-ray light scattering (SAXS) at the beamline 23A at the National Synchrotron Radiation Research Center (NSRRC) in Hsinchu, Taiwan. The intensity of the photon energy was operated

at about 10 keV. Samples were measured in a scattering vector (q-range) from 0.0025 to 0.1 $Å^{-1}$. The SAXS profiles were obtained at varying solid concentrations of PU dispersions in a range from 0.2 wt% to 30 wt% in different media (water, salt solution, or culture medium) incubated at 37 °C. The radius of gyration (R_g) in water was estimated by the Guinier analysis. The shape factor (R_g/ R_h) could be obtained from the values of R_h (D_h/2) and R_g.

2.3. Rheological measurements of the thermo-responsive sol-gel transition

The rheological properties of the PU dispersions of 25% solid concentration in the culture medium were measured by a rheometer (HR-2, TA Instruments, USA) with a cone and plate geometry. The cone used had a diameter of 40 mm and an angle of 2°. The sample (0.8 ml, 25 °C) was injected on the plate set at 37 °C. The concentration of the culture medium in the PU dispersions was exactly the same as that used for cell culture (HG-DMEM with sodium bicarbonate). The dynamic shear storage and loss modulus values were investigated at a constant frequency of 1 Hz and an 1% oscillatory strain against time. The steady state viscosity against different shear rates was measured by the static experiments, where the gel was in the same state as that used for co-extrusion experiments.

2.4. Culture of human dermal fibroblasts

The primary human dermal fibroblasts in this study were obtained from human adult foreskin after the surgery in the Tri-Service General Hospital, Republic of China (IRB#100–05–251). Human fibroblasts were isolated and expanded by an established procedure [23]. The tissues were digested by collagenase (No. C6885, Sigma-Aldrich), and the cell suspension was centrifuged, resuspended in the HG-DMEM supplement with sodium bicarbonate, 10% fetal bovine serum (FBS, Gibco, USA), and 1% penicillin-streptomycin (Invitrogen, USA), and incubated at 37 °C in a 5% CO_2 incubator. Cells were subcultured using 0.25% trypsin/EDTA solution (Gibco) after reaching 80% confluency. The medium was refreshed every three days. Forkhead box D3 (FoxD3) was a transcription factor and one of neural crest markers. The FoxD3 plasmid used in this experiment was obtained by reverse transcription polymerase chain reaction (RT-PCR) with EcoRV linkers was inserted into the pCR3.1 vector in frame with a FLAG tag [24]. The PolyFect reagent has branches with terminal amino groups, which are positively charged and can interact with negatively charged phosphate groups of nucleic acids. The concentration of FoxD3 plasmids in PU was 2 μg/ml for each transfection experiment.

2.5. FoxD3 transfection with the extrusion method and protein expression by immunofluorescent staining

The PU dispersion of 25% solid content in culture medium was preheated for 10 min at 60 °C first, then cooled down to 37 °C, and mixed with the cells and FoxD3 plasmid at 37 °C for 5 min before gelation. The density of human fibroblasts is 1×10^6/per ml in the final PU dispersion. After gelation for ~10 min, the cell-embedded PU gel was extruded through a 340 μm-size sterilized syringe needle to a 6-well plate. The shear rate of PU gel through the syringe needle was estimated based on Weissenberg-Rabinowitsch correction [25] and was about 220 s^{-1}. The fresh culture medium was added to the plate immediately. The plate was moved to the incubator. Meanwhile, the 2D-cultured fibroblasts transfected by the conventional method were employed for comparison. The conventional method to transfect the fibroblasts on the tissue culture plate (tissue culture polystyrene; TCPS) involved the use of the PolyFect reagent, and the detail was described in the previous study [8].

The delivery efficiency of FoxD3 into human fibroblasts was investigated by immunofluorescent staining at 24 h after extrusion. Anti-DDDDK tag antibody was used to detect FLAG fusion proteins (equivalent to FLAG antibodies). The hydrogel samples (with or without extrusion) were washed with phosphate buffered saline (PBS), fixed in 4% paraformaldehyde (PFA) solution for 30 min, and washed with PBS again to remove PFA. The samples were then treated with 0.1% Triton X-100 for 10 min and washed with PBS for permeation, blocked with 3% bovine serum albumin (BSA) for 1 h, and stained with anti-DDDDK tag antibodies (GTX115043, 1:200, Genetex, USA) at 4 °C overnight. After that, the samples were washed by PBS with Tween and incubated with a secondary FITC conjugated donkey anti-rabbit IgG antibody (Cat. 406416, 1:200, BioLegend, USA) at room temperature for 1 h, sealed, and examined by a fluorescence microscope. The excitation laser was a blue laser (488 nm) and the emission was green. Transfection efficiencies of FoxD3 were determined by dividing the number of fluorescent cells with the number of total cells. The total number of cells was estimated under the bright field. The number of positive cells was then estimated under the fluorescence in the same field of view. We randomly selected three fields of view to calculate the average transfection efficiency, and each of the experiment was performed for three times (i.e. an average from nine values). Additional experiments of a GFP plasmid (pEGFPC1, Addgene) were conducted to confirm if the immunofluorescence staining was due to unspecific binding of antibodies. GFP plasmids and human fibroblasts were co-extruded with the PU hydrogel with the similar shear stress (~190 Pa) and transfection efficiency was investigated after 24 h.

2.6. Cell viability

The viability of cells embedded in PU gel after extrusion was determined by staining with VitBright-48™ (VB-48), acridine orange (AO), and propidium iodide (PI) solution. The cell-laden hydrogel scaffolds were washed with PBS and stained with the VB-48/PI/AO tri-stain solution at the recommended concentration. After staining, cells were observed under the fluorescence microscope, and those displaying blue (VB-48-positive) and red (PI-positive) fluorescence represented viable and dead cells, respectively. Cell viability was presented as the population ratio of VB-48 positive cells. Further, the cell counting kit-8 (CCK-8, Sigma-Aldrich, Japan) assay was used to investigate cell proliferation in the long term. After *in situ* transfection by 3D printing for a certain period (0, 3, 7, and 14 days), each construct was washed and incubated with CCK-8 in the culture medium (CCK-8: culture medium = 1: 9) for 2 h at 37 °C. The supernatant was then transferred to a 96-well plate and was measured at 450 nm by a microplate reader (SpectraMax M5, Molecular Devices, USA). The value was deducted from the blank control (same construct without cells) and normalized to that of initial non-printed cells. The experiment was repeated for three times independently.

2.7. Neural differentiation of FoxD3 transfected cells in the hydrogel and gene expression

The cell-laden hydrogel samples and control groups (fibroblasts cultured on TCPS without transfection) were grown and induced for 14 days. To induce neural differentiation, the cell culture medium after two days was replaced by the neural differentiation medium [Neurobasal (Gibco), B27 supplement (Gibco), 1% penicillin, 20 ng/ml epidermal growth factor (Peprotech), and 40 ng/ml fibroblast growth factor 2 (Peprotech)] supplemented with Y27632 (20 μM) for 12 days [8,24]. The medium was refreshed

every three days. The total culturing time was 14 days before analyses.

For analysis of gene expression, the constructs were soaked in Trizol® reagent (Invitrogen, USA) and homogenized for RNA extraction. Total RNA of the hydrogel samples strand was reverse transcribed into cDNA and amplified by the RevertAidTM First Strand cDNA Synthesis Kit (MBI Fermentas, St. Leon-Rot, Germany). The quantitative reverse transcription-polymerase chain reaction (qRT-PCR) was performed using the DyNAmo Flash SYBR Green Qpcr Kit (Finnzymes Oy, Espoo, Finland) with succinate dehydrogenase complex flavoprotein subunit A (SDHA) as the housekeeping gene. All primer sequences used in this study are shown in Table S1, with annealing and extension temperature 60 °C. All experiments were conducted in triplicates. The expression of neural crest associated genes (FoxD3, Sox10), pluripotency associated genes (Oct4, Sox2, Nanog), and neural-associated genes [nestin, glial fibrillary acidic protein (GFAP), β-tubulin, microtubule-associated protein 2 (MAP-2)] were analyzed relative to the housekeeping gene SDHA and then normalized to the control group. The Delta-Delta Ct method to calculate the relative RNA expression was performed.

For the protein expression analyzed by Western blotting, the constructs were homogenized in RIPA lysis buffer [20 mM Hepes (pH 7.5), 420 mM NaCl, 1.5 mM $MgCl_2$, 0.1% NP-40, and protease inhibitor cocktail (Sigma)]. Sample protein concentrations were determined by the Bradford method. Sample proteins were separated by 10% and 6% sodium dodecyl sulfate polyacrylamide gel electrophoresis (SDS-PAGE) and then transferred to a polyvinylidene fluoride (PVDF) membrane. The membranes were washed and blocked in a 3% dry milk solution in PBS with 0.1% Triton X-100 for 1 h. Membranes were incubated with the primary antibodies (anti-GFAP Antibody, 840001, BioLegend; polyclonal nestin antibody, GTX116066; GeneTex; polyclonal β-tubulin antibody, 10,068-1-AP, proteintech; polyclonal GAPDH antibody, GTX100118, GeneTex) overnight at 4 °C, followed by incubation with secondary antibodies. The intensities of protein bands were detected by the Labwork software (UVP). The levels of each protein analyzed were normalized to the intensity values of GAPDH (loading control), and expressed as the fold of change over the control group.

2.8. Cell extrusion with the 3D bioprinter

A commercial 3D bioprinter (Regenovo, China) was used to perform the extrusion of human fibroblasts. Human fibroblasts with FoxD3 plasmid were mixed in the PU dispersion, with the density of cells 1×10^6 cells/ml and the solid content of PU 25%. The 3D bioprinter included an injection system with the computer and an x-y-z motion platform with a heater. The computer was used for design of the structure, planning of manufacturing paths, and motion control of the platform. The mixture of PU hydrogel was printed into a petri dish at 37 °C through a 410 μm sterilized syringe with ~80 kPa pressure in 8 mm/s. The shear rate used for printing was estimated by Weissenberg-Rabinowitsch correction and was about ~300 s^{-1}. The steady shear viscosity of PU1500 was ~1.3 Pa·s. The average shear stress generated by the 3D printer was estimated to be ~190 Pa, assuming laminar flow.

2.9. Statistical analysis

Multiple samples were gathered in each experiment. Each type of experiment was repeated for a minimum of three times independently. The data were expressed as mean ± standard deviation. Statistical analysis was performed with the ANOVA and Tukey post hoc test. Results were considered statistically significant when p values were <0.05.

3. Results

3.1. Synthesis and characterization of PU1500 nanoparticles

The PU1500 was successfully synthesized using an optimized procedure (as illustrated in Fig. S1). The ^{1}H NMR was used to determine the structure of the product. The characteristic peaks in the spectrum (represented as signals a–j) are shown in Fig. 1A. The peaks of triplet near 0.8 ppm and the peak near 3.6 ppm were assigned to the CH_3 group and CH_2 group in the component of IPDI [26], respectively. The peaks at 1.3–1.6, 2.2, and 4.0 ppm were assigned to the CH_2 group in PCL, and those at 1.5 and 5.2 ppm were assigned to the CH_3 and CH groups of PDLLA [27].

TEM images of PU nanoparticles are displayed in Fig. 1B. The nanoparticles revealed worm-like morphology. The average sizes obtained from the images were about 30–45 nm. Physicochemical characterization of PU nanoparticles (PU1500 and PU2000) and their molecular weights are shown in Table 1. The zeta potentials were below −30 mV, indicating stability of the PU nanoparticle dispersions. The values of hydrodynamic diameter (D_h or $2R_h$) were 30–40 nm, similar to the sizes obtained from TEM images. The values of R_g estimated from the SAXS experiment by Guinier analysis under low-q range was about 22 nm for both PUs. The shape factor (R_g/R_h) of PU1500 was ~1.41 and that of PU2000 was ~1.19. These values suggested a worm-like shape of the particles [28]. Based on the shape factors, PU1500 nanoparticles may be more rod-like than those of PU2000. The weight average molecular weight (M_w) of PU1500 and PU2000 determined by GPC was ~78 kDa and ~82 kDa, relatively close to each other.

3.2. The hydrogen bonding force and the crystallinity of PU

The extents of hydrogen bonding and crystallinity of PU evaluated by ATR-FTIR and XRD are demonstrated in Fig. 2. The characteristic IR peaks at 1730 cm^{-1} and 1647 cm^{-1} (Fig. 2A) each represented the free carbonyl group (C═O) and hydrogen-bonded (H-bonded) C═O in the structure. The proportion of H-bonded C═O group estimated from the spectra was 24.2% for PU1500, slightly higher than 20.1% for PU2000 [23]. After immersion in the culture medium, the H-bonded group increased in both PU1500 and PU2000. For PU1500, the increase in H-bonded C═O was obvious (from 24.2% to 36.7%), compared to the modest increase observed in PU2000 (from 20.1% to 21.5% [23]). This result indicated that PU1500 had more hydrogen bonding than PU2000 in the culture medium.

The XRD profiles were distinct between PU1500 and PU2000. When the soft segments of PU contained only PCL segments (2000 Da), the resulting PU was amorphous (Fig. S2). After 20 mol% of PCL segments were replaced by the same length of PDLLA segments (PU 2000), the crystalline PCL peaks at $2\theta = 21.21°$ and 23.51° showed up though PDLLA itself was amorphous (Fig. 2B). The crystallinity of PU2000 was quite impressive at 17.66%. However, PU1500 did not have any crystallinity, indicating that the PCL segments returned to amorphous state. These data suggested that PU1500 and PU2000, in spite of similar chemistry, may have very different microstructures. The amorphous structure of PU1500 (vs. the crystalline structure of PU2000) was confirmed by thermal analyses using TGA and DSC (Table S2).

3.3. Thermo-responsive properties and the effect of concentration in PU1500 dispersions

The thermo-responsive properties of PU1500 nanoparticle dispersion in water and in the culture medium are summarized in Table S3 and Fig. 3A. The diluted dispersion of PU1500 remained

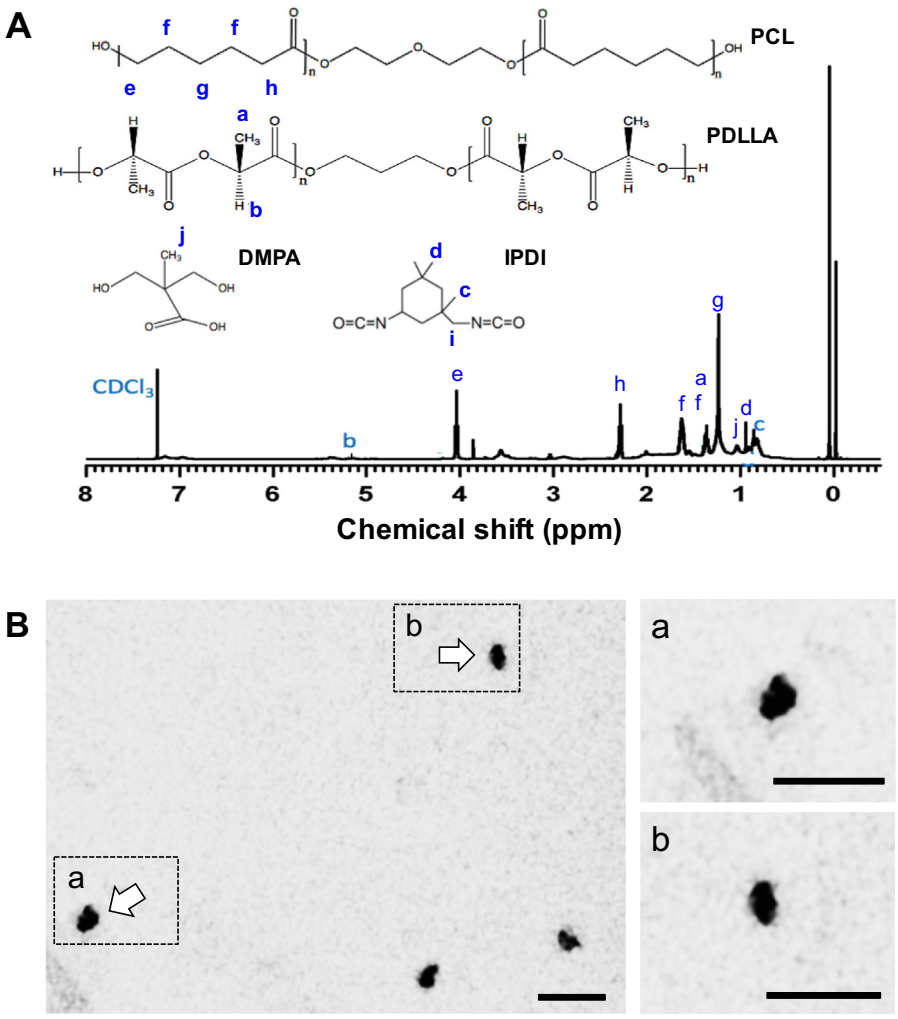

Fig. 1. Characterization of the newly synthesized PU (PU1500) nanoparticles. (A) ^{1}H NMR spectrum for PU1500. (B) TEM images for PU1500 NPs. The magnified images of selected NPs are indicated by boxes a and b, respectively. The average size calculated from TEM images was similar to that obtained from DLS. Scale bar, 100 nm.

Table 1
Characterization of PU1500 and PU2000 nanoparticles by DLS/SAXS/GPC.

PU NPs	DLS		SAXS	GPC	R_g/R_h (shape factor)
	D_h (nm) (=2R_h)	Zeta potential (mV)	R_g (nm)	M_w	
PU1500	30.8 ± 7.3	−43.0 ± 1.6	22.70	78028	1.41 (worm-like)
PU2000*	36.4 ± 0.8	−54.4 ± 2.0	21.60	82192	1.19 (worm-like)

* Ref. [21].

negatively charged and stable from 25 to 60 °C. When the temperature increased from 25 °C to 60 °C, the average D_h of PU1500 in water increased modestly from 30.8 nm to 32.8 nm, without statistically significant difference. While in the culture medium, the average D_h values increased from 30.6 nm to 39.6 nm as the temperature increased from 25 °C to 37 °C and further increased to 64.8 nm upon temperature increasing to 60 °C (Fig. 3A). The thermo-responsive properties of PU1500 nanoparticles were thus more pronounced in the culture medium vs. in water.

The SAXS profiles for PU1500 dispersions in different nanoparticle concentrations are shown in Fig. 3B and Fig. S3. There were four different concentrations of PU1500 (0.2, 1, 5, and 30%) dispersed in cell culture medium or in bicarbonate salt ($NaHCO_3$ only) solution at 37 °C. The hump position (black arrow) in the SAXS profiles represented the average size of the nanoparticles. There was no shift in the hump position (indicated by the black arrow) with different concentrations of PU1500. Meanwhile, a new hump (indicated by the white arrow) representing further arrangement of the structure showed up only at the higher solid content (30%). These results indicated that gelation of PU1500 dispersion depended on temperature, ions, as well as the solid content of the dispersion.

3.4. Rheological properties of the PU dispersions

Fig. 4(A–D) showed the dynamic rheological properties of the PU1500 and PU2000 dispersions in the culture medium at 37 °C against time. The sol-gel transition occurred at the point where the storage modulus (G′) and loss modulus (G″) intersected with

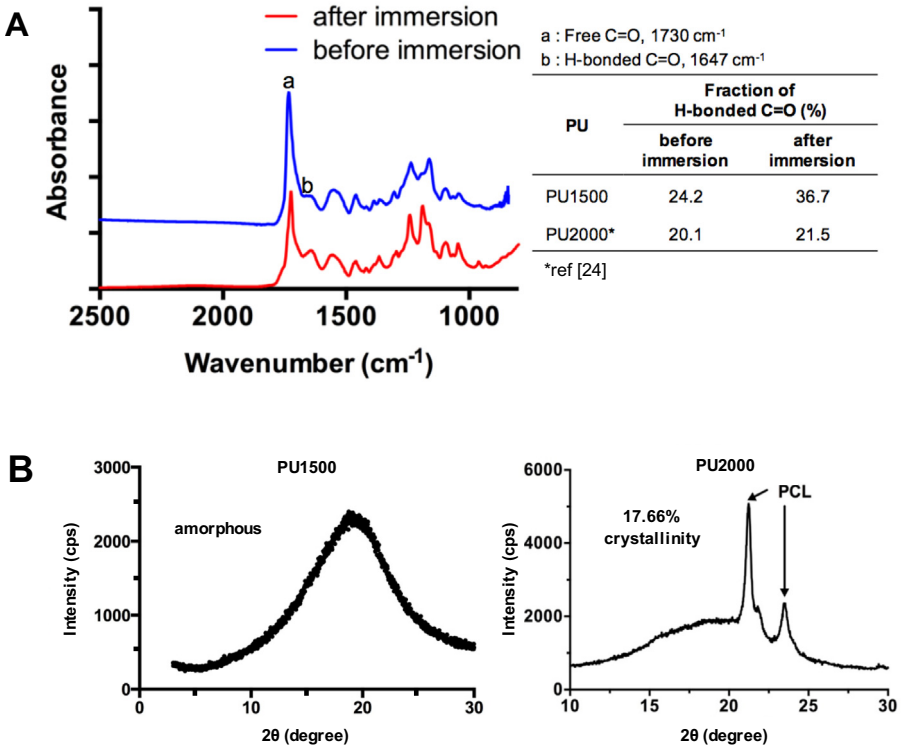

PU	Fraction of H-bonded C=O (%)	
	before immersion	after immersion
PU1500	24.2	36.7
PU2000*	20.1	21.5

*ref [24]

Fig. 2. Hydrogen bonding and crystallinity of PU1500 vs. PU2000. (A) ATR-IR spectra for PU1500 before and after immersion in the culture medium. The fraction of H-bonded C=O group was estimated based on the ratio of the peak areas for 1729 cm^{-1} and 1624 cm^{-1}, and compared with that previously reported for PU2000. (B) XRD profiles of PU1500 and PU2000. The total percentage of crystallinity estimated from the XRD peak areas in each PU is listed.

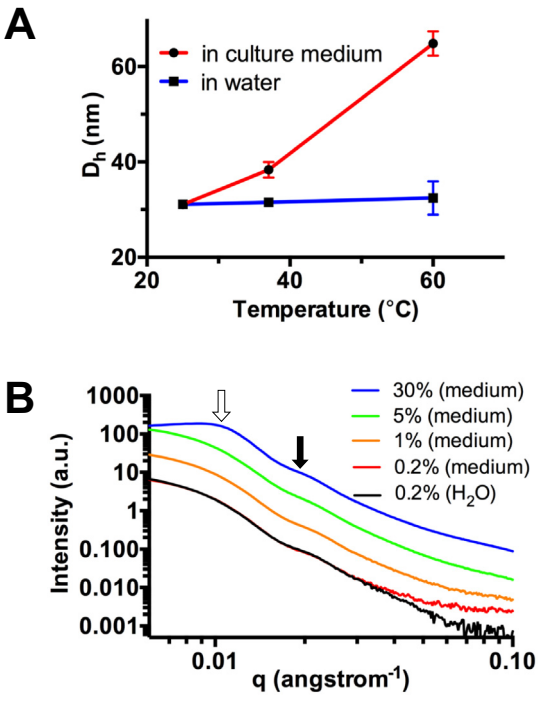

Fig. 3. Thermo-responsive property of PU1500 nanoparticle dispersion. (A) Hydrodynamic diameter (D_h) obtained by DLS for PU1500 diluted dispersion (2000 ppm) in water or in culture medium at various temperatures. (B) SAXS Profiles for PU1500 dispersions of various solid contents (0.2–30%) in culture medium at 37 °C. The black arrows correspond to the average size of the nanoparticles, and the white arrows indicate the inter-particle distance among the PU nanoparticles.

each other. The time to reach the transition is known as the gelation time. As shown in Fig. 4A and Fig. 4B, both of the PU dispersions (with 25% solid content) underwent sol-gel transition when placed at 37 °C. The gelation time of PU1500 was 1100 s, which was faster than PU2000 (2000 s). The gel modulus of PU1500 reached ~9000 Pa after 118 min, higher than that of PU2000 (~7200 Pa). The viscosity increase for PU1500 was also much faster vs. PU2000 (Fig. 4C and Fig. 4D). After 2000 s, the complex viscosity was 60 Pa·s for PU1500 and was only 2 Pa·s (30 times lower) for PU2000. These data indicated that the structure built up more quickly in PU1500. The steady shear viscosities against shear rates are demonstrated in Fig. 4E. For both PU1500 and PU2000, the steady shear viscosity decreased as the shear rate increased, i.e. with shear thinning properties. The steady shear viscosity at 220 s^{-1} (the approximate shear rate in the extrusion experiment) was ~1.5 Pa·s for PU1500 and ~0.4 Pa·s for PU2000. The respective average shear stress of the simple syringe extrusion was ~190 Pa for PU1500 and ~50 Pa for PU2000, assuming a state between plug flow and laminar flow.

3.5. FoxD3 transfection by the co-extrusion method in PU gel and the effect of transfection

FoxD3 plasmid was transfected to human fibroblasts by the extrusion method in PU1500 or PU2000 gel, as illustrated in Fig. 5. The dispersion was first pre-heated for 10 min, and then the human fibroblasts were mixed with the FoxD3 plasmid and the dispersion at 37 °C for 5 min before co-extrusion through the needle tip. The expression of FoxD3 in gel-embedded fibroblasts is demonstrated in Fig. 6, where the expression of FoxD3 was detected by the anti-DDDDK tag antibody and FITC conjugated secondary antibody. The expression of FoxD3, shown as the green flu-

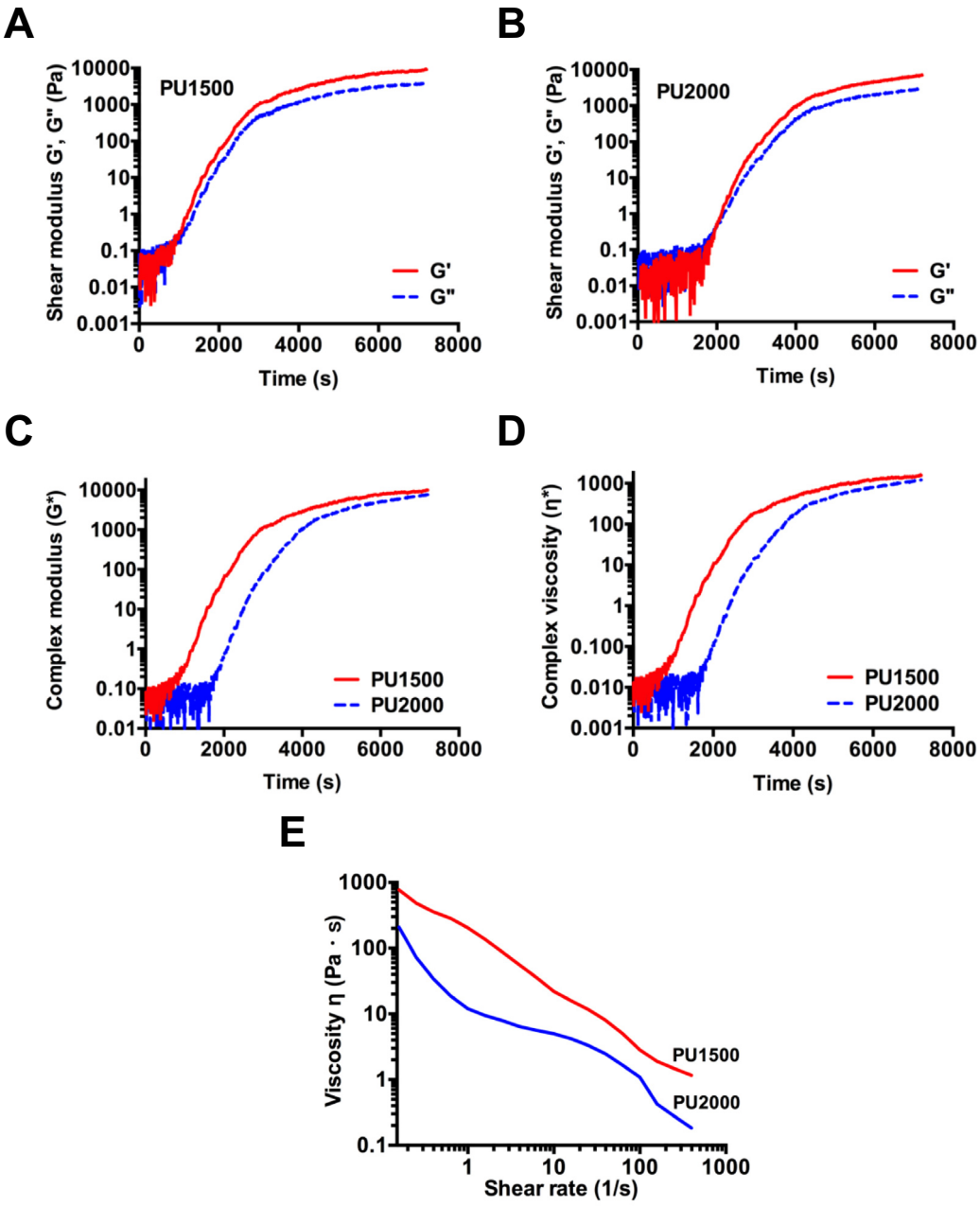

Fig. 4. Rheological properties of (A) PU1500 dispersion and (B) PU2000 dispersion against time at 37 °C, and a comparison of (C) the dynamic complex modulus, and (D) the dynamic complex viscosity. (E) The steady state viscosity of the two PU dispersions after incubation at 37 °C for 600 s.

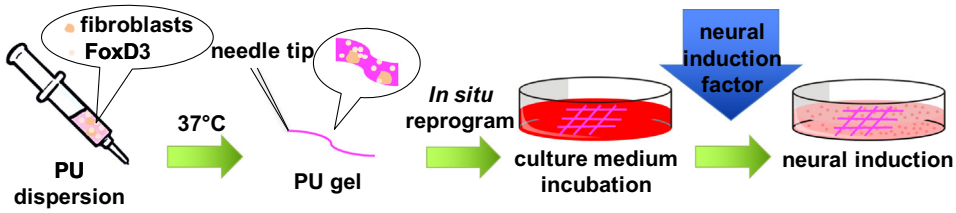

Fig. 5. Schematic diagram showing the *in situ* FoxD3 plasmid transfection of human fibroblasts by co-extrusion of the plasmids and cells with the PU hydrogel at 37 °C. The needle tip had a size of 340 μm.

orescence, was clearly observed in the extrusion group of PU1500 and PU2000. Not any fluorescent signal was observed in both control groups (without extrusion). With extrusion, the transfection efficiency was ~23.8% in the group of PU1500 and ~13.9% in the group of PU2000 after 24 h. The experimental analyses were performed on all cells, not the transfected cells. The cells and materials were printed and directly cultured. We also performed additional experiments using a GFP plasmid to confirm that the immunofluo-

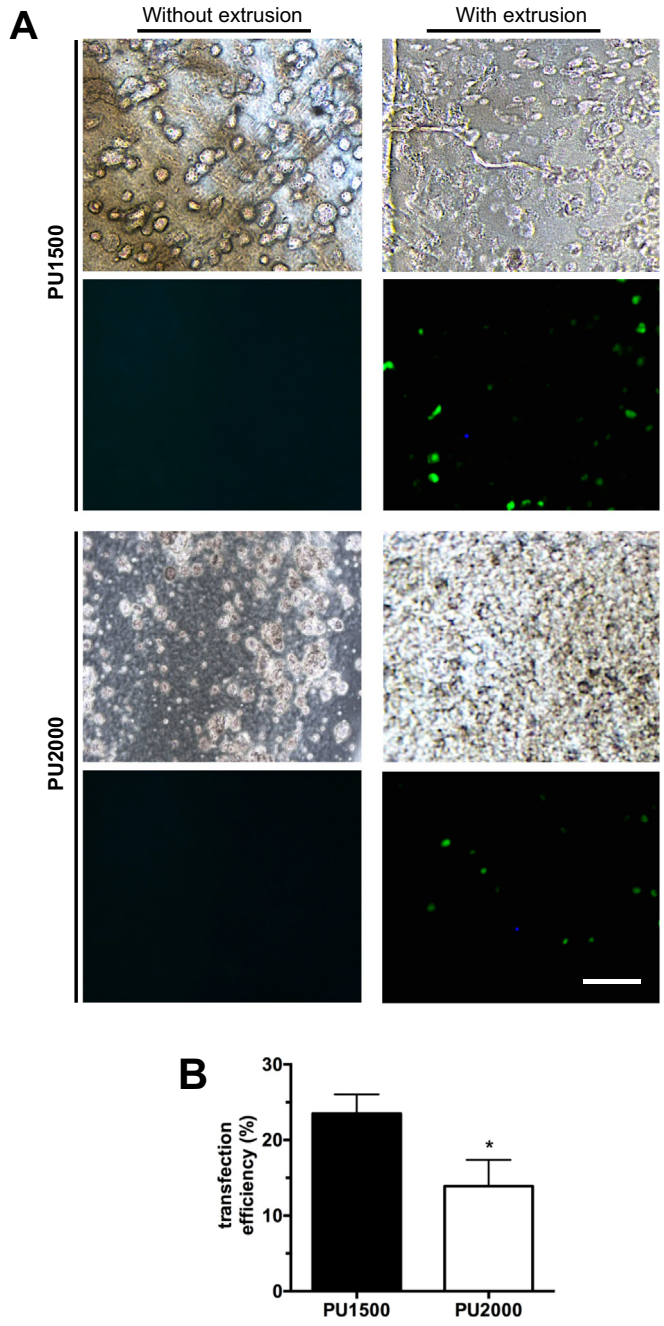

Fig. 6. The expression of exogenous FoxD3 in PU-embedded fibroblasts after extrusion and incubation for 24 h. (A) The expression of FoxD3 detected by immunostaining. FoxD3 plasmids and human fibroblasts were mixed in PU1500 or PU2000, and subjected (or not subjected) to extrusion as indicated. No signal was observed in both of the PU groups without extrusion. The transfection efficiency of FoxD3 was detected by immunostaining with anti-DDDDK tag antibody. (B) The transfection efficiency of fibroblasts after extrusion with FoxD3 plasmid in PU1500 and PU2000 at 24 h. The value observed in the control group was zero. Results are expressed as mean ± SEM, n = 3, $^{*}p < 0.05$. Scale bar, 50 μm.

rescence staining was not due to unspecific binding of antibodies. GFP plasmids and human fibroblasts were co-extruded with the PU hydrogel with the similar shear stress (~190 Pa). The transfection efficiency of GFP plasmid was found to be 20–30% (similar to that of FoxD3 plasmid, Fig. S4). This finding confirmed that the transfection efficiency was not caused by unspecific binding of antibodies. Taken together, these results indicated that FoxD3 could be successfully transfected into human fibroblasts by the PU gel extrusion method. Besides, the transfection efficiency was different for different hydrogels used in co-extrusion and depended on shear stress generated by 3D printing. Using PU1500 for extrusion gave rise to a greater transfection efficiency than using PU2000. Various shear stresses could be generated by 3D printing (~40, 190, and 250 Pa). The transfection efficiency at 190 Pa was close to that obtained by the simple syringe extrusion. The transfection efficiency at the higher shear stress (~250 Pa) was greater (averaged 28.6%) and at the lower shear stress (~40 Pa) was lower (averaged 10.5%), compared to 190 Pa (24%). The positive correlation of transfection efficiency and average shear stress is demonstrated in Fig. S5(A, B).

3.6. The viability of fibroblasts after extrusion with PU gel

Viable cells in the extruded PU1500 gel could be visualized by VB-48 staining, as illustrated in Fig. 7A. These images showed the apoptotic cells stained with PI (red color) and the healthy cells stained with VB-48 (blue color). The bright field was used to identify all cells. The apparent color of VB-48 images was between blue and green. We assumed that this was an influence from the strong green fluorescence background of PU in the surrounding. The viability was calculated from the number of viable cells divided by the number of all cells. The average cell viability was about 65% after extrusion for transfection, and there was no significant decrease in cell viability in 72 h. The viability of cells directly transfected in PU1500 gel compared to those transfected first with the conventional PolyFect reagent and then extruded in PU1500 gel is shown in Fig. 7C, using fibroblasts extruded in gel without plasmid as the control group. There was no obvious difference in the cell viability between the control group and the group extruded with plasmid. Meanwhile, the PolyFect transfected group showed lower viability below 50%. Therefore, the shear force of the extrusion caused the death of some human fibroblasts in particular for the PolyFect-transfected ones. The long term viability of human fibroblasts after *in situ* transfection by 3D printing was also evaluated and is presented in Fig. 7D. Three different shear stresses were used to compare one another. When a higher shear stress (~250 Pa) was used for the printing, the transfection efficiency increased but the survival rate also decreased (~50%). In addition, cell proliferation or cell number recovery during the 14 day culture period was not significant. These results were in contrast to the lower shear stress (~40 Pa) group (90% viability). Moreover, the number of cells printed under the shear stress finally employed in this study (i.e. ~190 Pa, ~65% survival) recovered significantly from 3 to 7 days, reaching ~85% at 7 days. While the culturing time increased to 14 days, the cell number increased to above 90%.

3.7. The expression of associated genes of neural crest and stemness genes after extrusion, and neural lineage-related markers after induction

The fibroblasts transfected with FoxD3 by the extrusion method were analyzed for the gene expression of neural crest transcription factors and stemness transcription factors, shown in Fig. 8A and Fig. 8B. The representative genes of neural crest are FoxD3 and Sox10 [29]. The neural crest cells were considered as the multipotent stem cells with differentiation characteristics. The Oct4, Sox2, and Nanog genes are representative genes of stem cells [30]. Upregulation of these markers in human fibroblasts indicated their reprogramming into neural crest cells [8]. The expression of FoxD3 and Sox10 genes was upregulated for both PU1500 and PU2000 transfected groups than the non-transfected control group (fibroblasts cultured on TCPS without transfection). The gene expression of stemness markers Oct4, Sox2, and Nanog also followed the same trend. The conventional transfection reagent (PolyFect) was used

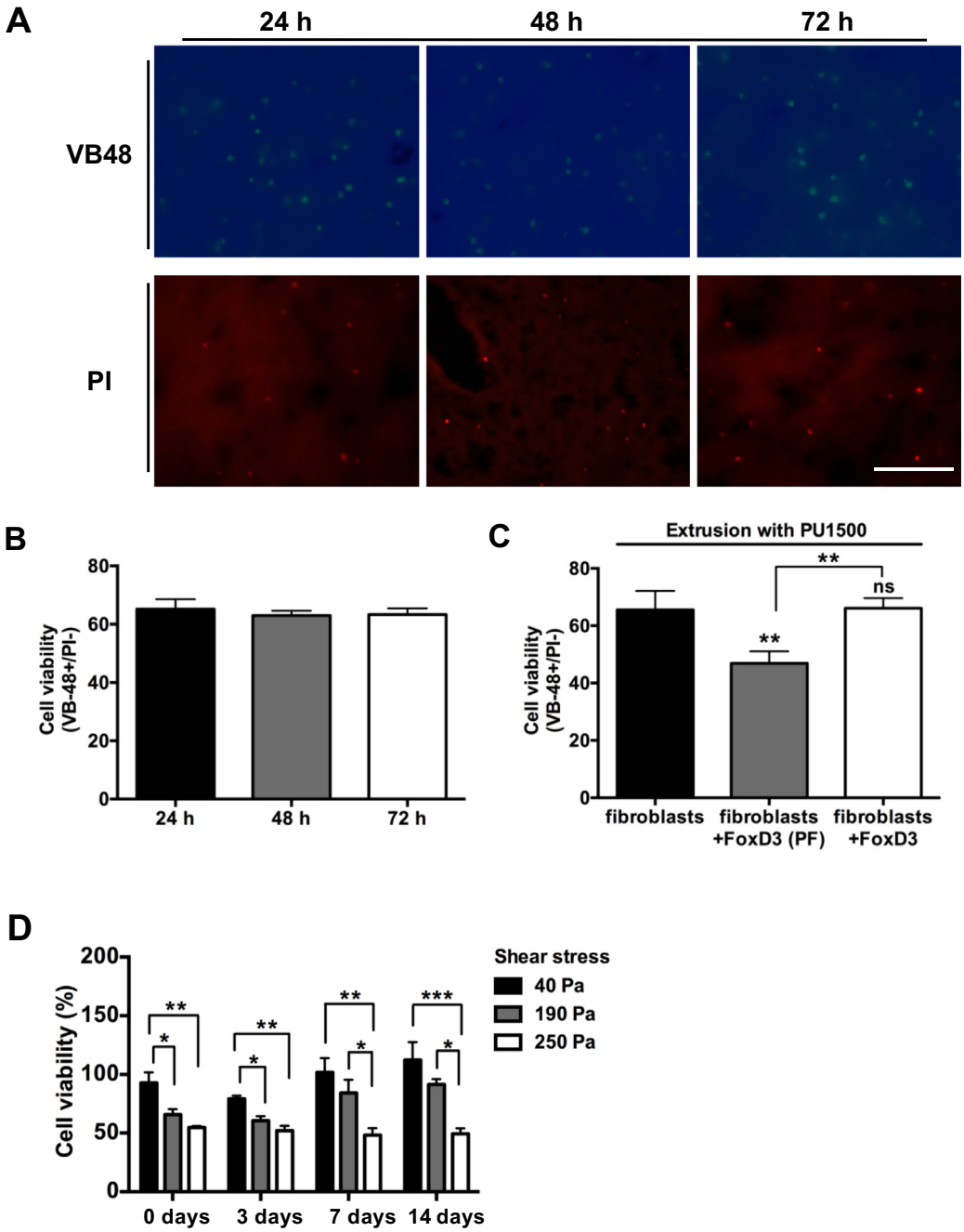

Fig. 7. The viability of fibroblasts after extrusion with PU1500. (A) Images of healthy cells and apoptotic cells were determined using VitaBright Stains after extrusion with FoxD3 plasmid in PU1500 at 24 h, 48 h, and 72 h. The dead cells were stained red with PI, and the healthy cells were stained blue with VB-48. (B) The viability of fibroblasts after extrusion with FoxD3 plasmid in PU1500 was presented as the percentages of VB+/PI− cells at 24 h, 48 h, and 72 h. (C) The viability of fibroblasts after transfection by the conventional PolyFect or by *in situ* PU co-extrusion at 24 h. In PolyFect group, the cells were transfected with FoxD3 using PolyFect on TCPS, selected for live cells and later extruded with PU1500. (D) Long-term cell viability by the *in situ* transfection using 3D printing of in different shear stresses, evaluated by CCK-8. The viability was deducted from the blank control (i.e. the PU construct without cells), normalized to that of initial (non-printed) cells. Scale bar, 100 μm. Results are expressed as mean ± SD (n = 3). $^{**}p < 0.01$, ns = no significance, among the indicated groups. (For interpretation of the references to color in this figure legend, the reader is referred to the web version of this article.)

as the standard transfection method in this comparative analysis. Cells were extruded in PU gel after conventional transfection by PolyFect for comparison. The data were represented by "PF". These cells had higher FoxD3 but lower Sox10 and Oct4 gene expression.

The expression of neural lineage-related genes for the constructs at 14 days is demonstrated in Fig. 8C. The expression of nestin and β-tubulin genes was significantly higher for all FoxD3 transfected groups. The gene expression of GFAP, MAP-2 and β-tubulin in the PU1500 transfected and PolyFect transfected groups was higher than that in the PU2000 transfected group. Meanwhile, the GFAP expression in PU2000 was low and not significantly different from the control. These results suggested that human fibroblasts co-extruded with FoxD3 plasmid in PU gel may be

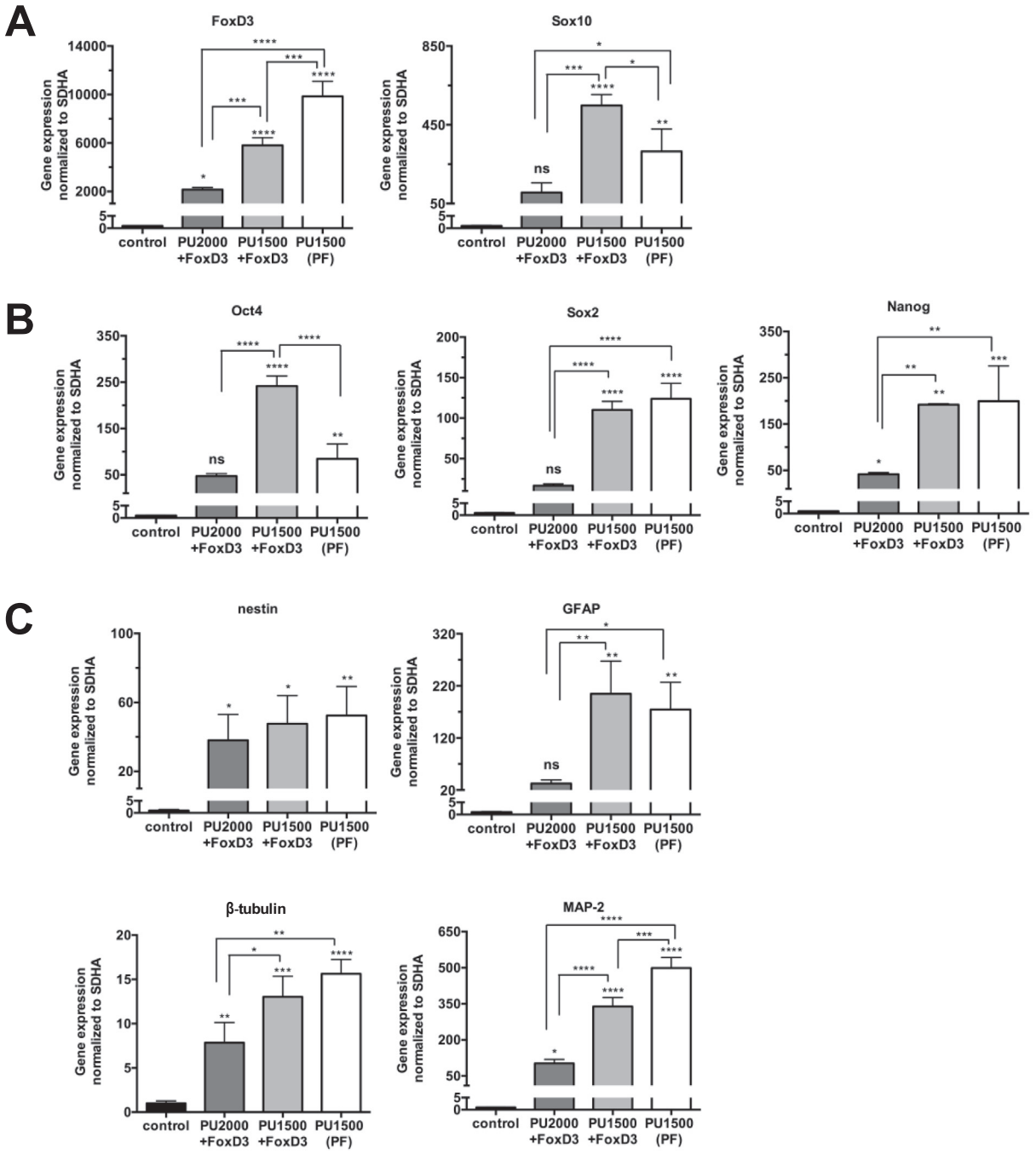

Fig. 8. The gene expression of fibroblasts transfected with FoxD3 by the *in situ* PU co-extrusion method or by the PolyFect transfection method, determined by qRT-PCR. The expression of (A) neural crest associated genes and (B) stemness associated genes after transfection and culture for 3 days. (C) The expression of genes related to neural lineages, nestin, GFAP, β-tubulin, and MAP-2 after transfection, culture, and neural induction for 14 days. PF indicates the PolyFect transfected group. Control indicates fibroblasts on TCPS without transfection (A, B) in basal medium (without induction) or in neural induction medium (C). Results are expressed as mean ± SD (n = 3). $^{*}p < 0.05$; $^{**}p < 0.01$; $^{***}p < 0.001$; $^{****}p < 0.0001$, ns = no significance, among the indicated groups.

reprogrammed into neural crest stem cells and differentiate into neural lineages after the neural induction.

3.8. Cell-laden constructs fabricated by the 3D bioprinter and gene expression

The PU1500 hydrogel were used as a bioink to print cell-laden constructs, as shown in Fig. 9A. The cell/plasmid/gel mixture was dispensed at the constant speed of 8 mm/s at 37 °C. At this optimized condition, the shear rate was about 300 s^{-1} and the corresponding steady shear viscosity was ~1.3 Pa·s. The average shear stress was estimated to be ~190 Pa. Constructs with a dimension of 20 mm × 20 mm × 5 mm were printed on sterile glass coverslip and transferred to 6-well culture plates. The results are shown in Fig. 9B and Fig. 9C. The neural crest and stemness marker genes were upregulated in both syringe extrusion and 3D printing groups over the control group (Fig. 9B). After neural induction, the gene expressions of neural-related markers at 14 days for cells printed

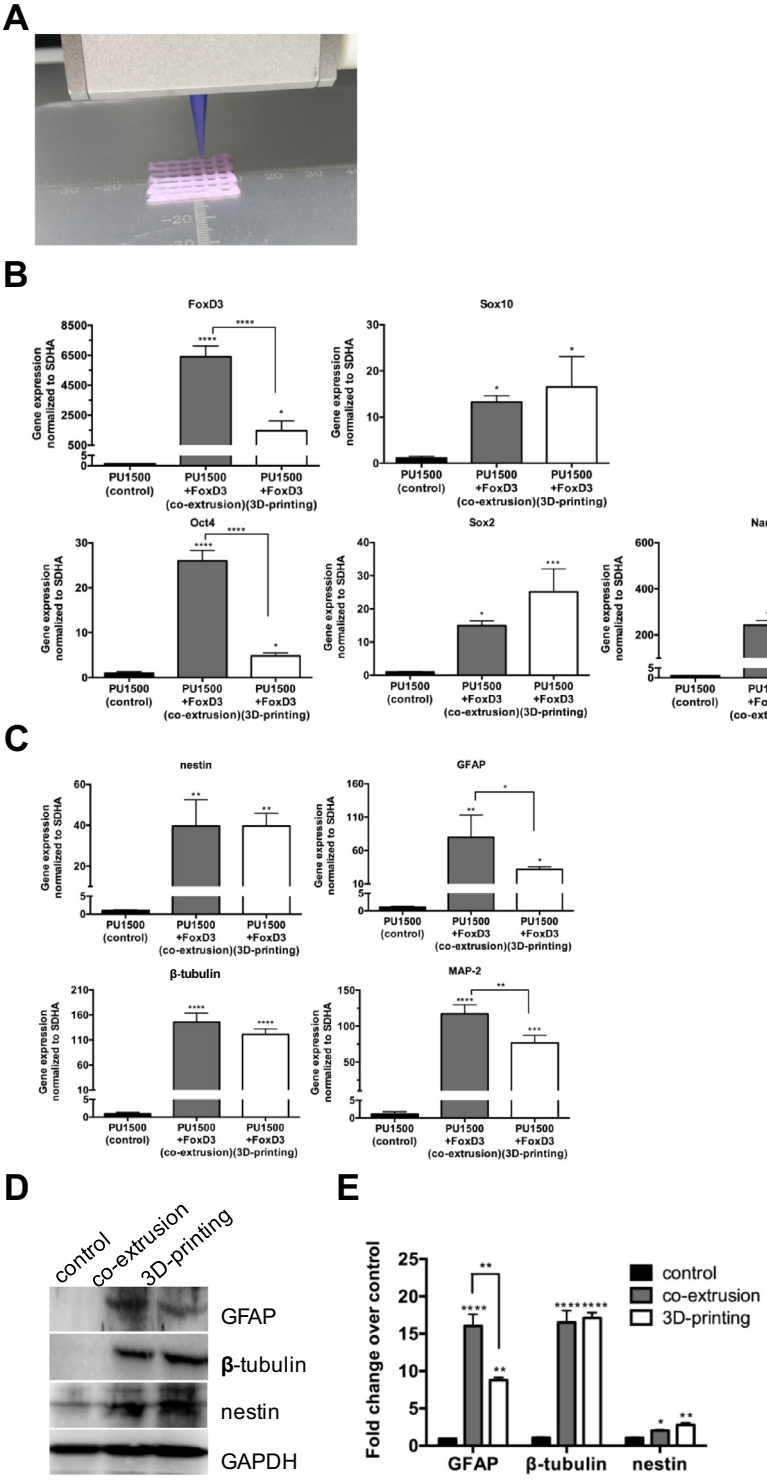

Fig. 9. 3D printed cell-laden constructs. (A) Human fibroblasts were embedded in PU1500 hydrogel and printed at 37 °C by the commercial extrusion-based 3D bioprinter. The scaffold size was 20 × 20 × 0.5 mm, and the needle tip had a size of 410 μm. (B) The gene expression of stemness associated markers after printing and before neural induction, and (C) the gene expression of neural lineage markers of neural induction at 14 days. "Co-extrusion" refers to the syringe extrusion (non-printed) method. "3D-bioprinting" refers to the extrusion-based 3D printing. "Control" indicates fibroblasts without transfection in PU1500 hydrogel. (D) Representative Western blots showing the expression of GFAP, β-tubulin, and nestin in the co-extrusion and 3D-printing groups in comparison to the control group. (E) Semi-quantitative analyses of protein levels normalized to GAPDH and expressed as the fold of change over control. Results are expressed as mean ± SD (n = 3). $^{*}p < 0.05$; $^{**}p < 0.01$; $^{***}p < 0.001$; $^{****}p < 0.0001$, among the indicated groups.

with PU1500 were still greater than extrusion with PU2000 (data not shown), but were equal or slightly less than those obtained with the simple syringe extrusion (non-printed) method. To further verify the protein expression of neural lineage-related markers, Western blots for constructs at 14 days were performed and the data are demonstrated in Fig. 9D. The expression of differentiated marker proteins (GFAP and β-tubulin) was significantly upregulated in both syringe extrusion and 3D printing groups

but not in the control group. The tendency of protein expression was consistent with that of gene expression at 14 days (Fig. 9E).

4. Discussion

Strategies to directly transfect cells by applying temporary external force have been reported recently. A microfluidic platform that brings cells through a constrictive passage may deliver substances into the cells [19]. Plasmids encoding GFP were co-printed with porcine aortic endothelial (PAE) cells through an inkjet printer [31]. Multipotent stromal cells (MSCs) co-printed with plasmid DNA encoding BMP-2 in alginate hydrogel as ~840 μm thick fibers were differentiated into the osteogenic lineage [32]. These processes may induce transient permeability on cell membranes. However, the literature was still limited and the shear stress exerted by these processes was not examined. Moreover, there is no study so far on cell reprogramming *in situ* with 3D bioprinting. Here, we tried to develop a bioink (material) and bioprinting process that could be used to print human fibroblasts into personalized tissue constructs, particularly for neural-related applications.

Two different thermo-responsive PU (PU1500 and PU2000) dispersions with different molecular weight of PDLLA diol in the soft segment were compared in this study for their printing and reprogramming abilities. The R_h of PU1500 in cell culture medium increased significantly when the temperature was raised from 25 °C to 60 °C. As the temperature increased, the molecular chains of the PU nanoparticles might become more mobile. The water molecule then could penetrate the PU nanoparticles and cause the swelling [26]. In the environment of cell culture medium, the Na^+ ions dissociated from the culture medium may interact with $–COO^-$ in the hard segment, resulting in more swelling of the nanoparticles. The shape factor of PU nanoparticles (R_g/R_h) was 1.41 for PU1500 and 1.19 for PU2000. The value of shape factor for homogenous sphere-like nanoparticles was ~0.7 and that for rod-like nanoparticles was ~1.5 [33]. Therefore, the shape of PU1500 nanoparticles was more elongated than PU2000. Nanoparticles which are more rod-like may be more easily packed among one another than sphere-like nanoparticles [34]. The more compact and densely packed PU1500 thus had larger elastic modulus than PU2000. Because the PU particles are not micelles, the sizes obtained from TEM and DLS were similar [26]. The ATR-IR spectra supported more hydrogen bonding of carbonyl group for PU1500, which also suggested a greater degree of microphase separation for PU1500 [35]. The greater secondary force in PU1500 may enhance chain-folding and swelling [36].

Gelation occurs in a wide range of hydrogel systems where particles attract with each other [37]. PU1500 with the greater nanoparticle interaction force may form gel more quickly, which was confirmed by rheology. According to the SAXS profiles of the nanoparticle dispersion, a slight peak in the low-q region appeared at the solid content of 30%, indicating the aggregation or clustering of the nanoparticles. The rate of aggregation increased with the increased particle concentration [38]. When nanoparticles started to aggregate, the secondary force interaction including the hydrogen bond contributed to sol-gel transition. In our previous findings, the amorphous PDLLA with M_n 2000 Da in the PU2000 caused PCL segments to crystallize [21]. Unlike PU2000, the more easily gelled PU1500 did not show any crystallinity of PCL segment based on XRD profiles. Therefore, soft segment crystallization was not a pre-requisite for PU nanoparticle dispersion to undergo gelation, though most previous studies proposed the gelation highly correlated with soft segment crystallinity [21,26].

The shear stress and compressive force produced by extrusion during the printing process are important because they should be large enough to induce cell permeability but small enough not to disrupt the cell membrane [22]. Transfection via the extrusion method by 3D bioprinting was a simpler, more convenient, and faster way than most of the transfection methods. The transfection was achieved *in situ* and followed by regular culture, while the process of conventional transfection by PolyFect actually took longer than 3 days. We believed that the PU gel with viscoelastic properties could provide the squeezing effect to the co-extruded cells through the syringe needle tip. Results showed that the transfection efficiency by extrusion with PU1500 was higher than that with PU2000. Both PUs had shear-thinning properties. As mentioned (Sec. 3.4.), the average shear stress in PU1500 was estimated to be ~190 Pa, which was higher than ~50 Pa in PU2000. In literature, the shear stress values for substance delivery was in the order of 100 Pa for shear exposure times in minutes [39]. On the other hand, the shear rate produced by 3D bioprinting of PU1500 through the commercial extrusion-based 3D printer could be adjusted by air pressure and the average shear stress was selected near 190 Pa (close to that produced by simple extrusion). Therefore, the transfection effect remained similar between simple syringe extrusion and 3D printing under the close shear stress. Comparing the shear stress values and the transfection efficiency between PU1500 and PU2000, it was evident that the rheological properties of the bioink determined the reprogramming efficiency. Moreover, the constructs from PU1500 had better neural associated marker expression than those from PU2000, including nestin, GFAP, β-tubulin, and MAP-2. Meanwhile, the difference in the transfection efficiency and gene expression between the simple extruded and printed PU1500 groups may be ascribed to the difference in the shear exposure time, which was shorter for the printed constructs.

According to our previous data, the actual yields of PolyFect-mediated and chitosan-based transfection methods were 22.4% and 12.4%, respectively [8]. The yield of *in situ* transfection by 3D printing was 15.6% (i.e. 24% × 65%). The *in situ* transfection by 3D printing was thus more effective than the chitosan-based transfection method, plus the cells were printed. Besides, this yield (15.6%) was greater than that of 2D transfection followed by extrusion for printing (14%). Furthermore, our long-term cell viability data (by the CCK-8 assay) showed that the cell number was recovered to ~85% after *in vitro* culture for 7 days. The shear stress of printing could be controlled and optimized to promote the transfection efficiency. Although shear thinning materials often result in relatively lower cell viability after printing because of the shear force induced cell injury [40], the number of viable cells was rescued after culture in this study. The shear stress finally employed in this study (i.e. ~190 Pa, with ~65% cell survival) was appropriate to print the structure from the PU hydrogel. The cells in hydrogel printed with a lower shear stress (~40 Pa) did not have satisfactory transfection while those with a higher shear stress (~250 Pa) did not survive well and the cell number was not rescued after 14 days. The hydrogel printed at the lower or higher stresses did not possess continuous structure either. We expect to regulate the rheological properties to expand the working window of PU hydrogel, and add the antioxidant or growth factor to further enhance the cell survival and proliferation in PU hydrogel.

The *in situ* reprogramming by 3D bioprinting provides a number of potential advantages over existing methods. The method had better cell viability and higher throughput than electroporation [41] and microinjection [42]. Although the influence of each factor (needle tip size, extrusion time, etc.) on the transfection and reprogramming efficiency were not fully defined yet, we have demonstrated that human fibroblasts could be reprogrammed into neural crest-like stem cells with FoxD3 plasmid by 3D bioprinting, and the reprogrammed cells could undergo neural differentiation in the printed structure after induction. In addition, neural cells

co-grafted with fibroblasts may enhance axonal regeneration, and may adhere to the fibroblasts as well as the extracellular matrix produced by the fibroblasts [43,44]. Moreover, our previous study showed that the FoxD3 reprogrammed fibroblasts (chitosan-based transfection with a yield 12.4%) could regenerate the nervous system injury of adult zebrafish [8]. These might suggest that the presence of non-reprogrammed fibroblasts in the construct may be advantageous to neural regeneration. It is also possible to incorporate the induction factor in the bioink for printing the customized neural tissues from fibroblasts. Finally, it is necessary to improve the function of the regenerated neural-like tissue for applications in tissue repair and drug screening in the future.

5. Conclusions

A new thermo-responsive PU hydrogel (PU1500) was synthesized and characterized in this study. The elasticity of the PU hydrogel was intended to induce a transfection effect when used as ink for 3D cell printing. When the PU was extruded through the needle tip, the shear stress (~190 Pa) and shear rate (200–300 s^{-1}) may cause the transient membrane permeability for transfection without the toxic effect of conventional transfection reagents. To show that this method could be used to directly reprogram the printed cells, FoxD3 plasmids were co-printed with FoxD3 plasmids in PU hydrogel. The expression of exogenous FoxD3 was significantly dependent on the rheological properties of the PU hydrogel. PU1500 hydrogel with a greater extent of hydrogen bonding and higher viscoelasticity had better reprogramming effect than the previously reported PU2000 hydrogel. Meanwhile, the transfection by extrusion in PU1500 gel was similar in efficiency as the conventional transfection reagent (PolyFect) but higher in cell viability. Human fibroblasts reprogrammed with FoxD3 *in situ* by 3D bioprinting could differentiate into neural-like cells after culture and induction for 14 days. The neural-like tissue engineering constructs fabricated from human fibroblasts co-printed with FoxD3 plasmids in PU hydrogel may be applied for neuroregeneration or further developed as mini-brain for basic research and drug screening.

Acknowledgements

This work was funded by the Program Project for Regenerative Medicine (106–3114–Y–043–021; 106–3114–B–002–008), Ministry of Science and Technology, Taiwan, and partially supported by the institutional resources including National Health Research Institutes (Central Government S & T Grant, Taiwan 107-0324-01-19-03) as well as National Taiwan University (Cutting-Edge Steering Research Project NTU–CESRP–106R7626). FoxD3 expression plasmids were kindly provided by Dr. Duanqing Pei (Guangzhou Institutes of Biomedicine and Health, Guangzhou, P. R. China). Dermal fibroblasts were generously supplied by Dr. Niann-Tzyy Dai (Tri-Service General Hospital, Taipei, Republic of China). We also thank National Synchrotron Radiation Research Center (2017–2–183–1) and the staffs, particularly, Dr. U-Ser Jeng for providing the resources and technical support.

Appendix A. Supplementary data

Supplementary data associated with this article can be found, in the online version, at https://doi.org/10.1016/j.actbio.2018.01.044.

References

[1] A.J. Stoessl, Gene therapy for Parkinson's disease: a step closer?, Lancet 383 (2014) 1107–1109
[2] N. Picard-Riera, B. Nait-Oumesmar, A. Baron-Van, Evercooren, Endogenous adult neural stem cells: limits and potential to repair the injured central nervous system, J. Neurosci. Res. 76 (2) (2004) 223–231.
[3] K. Takahashi, K. Okita, M. Nakagawa, S. Yamanaka, Induction of pluripotent stem cells from fibroblast cultures, Nat. Protoc. 2 (12) (2007) 3081–3089.
[4] D.X. Yu, M.C. Marchetto, F.H. Gage, Therapeutic translation of iPSCs for treating neurological disease, Cell Stem Cell 12 (6) (2013) 678–688.
[5] B.Y. Hu, J.P. Weick, J. Yu, L.X. Ma, X.Q. Zhang, J.A. Thomson, S.C. Zhang, Neural differentiation of human induced pluripotent stem cells follows developmental principles but with variable potency, Proc. Natl. Acad. Sci. U. S.A. 107 (9) (2010) 4335–4340.
[6] M. Denham, M. Dottori, Neural differentiation of induced pluripotent stem cells, Methods Mol. Biol. 793 (2011) 99–110.
[7] E. Lujan, M. Wernig, The many roads to Rome: induction of neural precursor cells from fibroblasts, Curr. Opin. Genet. Dev. 22 (5) (2012) 517–522.
[8] T.C. Tseng, F.Y. Hsieh, N.T. Dai, S.H. Hsu, Substrate-mediated reprogramming of human fibroblasts into neural crest stem-like cells and their applications in neural repair, Biomaterials 102 (2016) 148–161.
[9] R. Waehler, S.J. Russell, D.T. Curiel, Engineering targeted viral vectors for gene therapy, Nat. Rev. Genet. 8 (8) (2007) 573–587.
[10] Y.C. Hu, Baculoviral vectors for gene delivery: A review, Curr. Gene Ther. 8 (1) (2008) 54–65.
[11] I.I. Slowing, B.G. Trewyn, V.S.Y. Lin, Mesoporous silica nanoparticles for intracellular delivery of membrane-impermeable proteins, J. Am. Chem. Soc. 129 (28) (2007) 8845–8849.
[12] D.W. Pack, A.S. Hoffman, S. Pun, P.S. Stayton, Design and development of polymers for gene delivery, Nat. Rev. Drug Discov. 4 (7) (2005) 581–593.
[13] J. Zabner, Cationic lipids used in gene transfer, Adv. Drug Deliv. Rev. 27 (1) (1997) 17–28.
[14] S. Li, Electroporation gene therapy: new developments in vivo and in vitro, Curr. Gene Ther. 4 (3) (2004) 309–316.
[15] M.B. Fox, D.C. Esveld, A. Valero, R. Luttge, H.C. Mastwijk, P.V. Bartels, A. van den Berg, R.M. Boom, Electroporation of cells in microfluidic devices: a review, Anal. Bioanal. Chem. 385 (3) (2006) 474–485.
[16] Y. Zhang, L.C. Yu, Microinjection as a tool of mechanical delivery, Curr. Opin. Biotechnol. 19 (5) (2008) 506–510.
[17] D. Luo, W.M. Saltzman, Synthetic DNA delivery systems, Nat. Biotechnol. 18 (1) (2000) 33–37.
[18] D.L. Miller, S.V. Pislaru, J.E. Greenleaf, Sonoporation: mechanical DNA delivery by ultrasonic cavitation, Somat. Cell Mol. Genet. 27 (1–6) (2002) 115–134.
[19] A. Sharei, J. Zoldan, A. Adamo, W.Y. Sim, N. Cho, E. Jackson, S. Mao, S. Schneider, M. Han, L.J. Abigail, P.A. Basto, S. Jhunjhunwala, J. Lee, D.A. Heller, J.W. Kang, G. C. Hartoularos, K. Kim, D.G. Anderson, R. Langer, K.F. Jensen, A vector-free microfluidic platform for intracellular delivery, PNAS 110 (6) (2013) 2082–2087.
[20] X. Cui, D. Dean, Z.M. Ruggeri, T. Boland, Cell Damage Evaluation of Thermal Inkjet Printed Chinese Hamster Ovary Cells, Biotechnol. Bioeng. 106 (6) (2010) 963–969.
[21] H.H. Lin, F.Y. Hsieh, C.S. Tseng, S.H. Hsu, Preparation and characterization of a biodegradable polyurethane hydrogel and the hybrid gel with soy protein for 3D cell-laden bioprinting, J. Mater. Chem. B 4 (2016) 6694–6705.
[22] S.H. Hsu, K.C. Hung, Y.Y. Lin, C.H. Su, H.Y. Yeh, U.S. Jeng, C.Y. Lu, S.A. Dai, W.E. Fu, J.C. Lin, Water-based synthesis and processing of novel biodegradable elastomers for medical applications, J. Mater. Chem. B 2 (2014) 5083–5092.
[23] Y.H. Lin, K.Y. Fu, P.D. Hong, H. Ma, N.H. Liou, K.H. Ma, J.C. Liu, K.L. Huang, L.G. Dai, S.C. Chang, J. Yi-Hsin Chan, S.G. Chen, T.M. Chen, N.T. Dai, The effects of microenvironment on wound healing by keratinocytes derived from mesenchymal stem cells, Ann. Plast. Surg. 71 (Suppl. 1) (2013) S67–S74.
[24] K. Hirano, S. Nagata, S. Yamaguchi, M. Nakagawa, K. Okita, H. Kotera, J. Ainscough, T. Tada, Human and mouse induced pluripotent stem cells are differentiatlly reprogrammed in response to kinasa inhibitors, Stem Cell Dev. 21 (2012) 1287–1298.
[25] J.A. King, F.A. Morrison, J.M. Keith, M.G. Miller, R.C. Smith, M. Cruz, A.M. Neuhalfen, R.L. Barton, Electrical Conductivity and Rheology of Carbon-Filled Liquid Crystal Polymer Composites, J. Appl. Polym. Sci. 101 (2006) 2680–2688.
[26] C.W. Ou, S.C.H. Su, U.S. Jeng, S.H. Hsu, Characterization of biodegradable polyurethane nanoparticles and thermally induced self-Assembly in water dispersion, ACS Appl. Mater. Interfaces 6 (2014) 5685–5694.
[27] C.D.C. Erbetta, R.J. Alves, J.M. Resende, R.F.D.S. Freitas, R.G.D. Sousa, Synthesis and characterization of poly(D, L-Lactide-co-Glycolide) copolymer, J. Biomater. Nanobiotechnol. 3 (2012) 208–225.
[28] K.L. Hammer, M.M. Maye, Thermal aggregation properties of nanoparticles modified with temperature sensitive copolymers, Langmuir 29 (2013) 15217–15223.
[29] S.M. Honoré, M.J. Aybar, R. Mayor, Sox10 is required for the early development of the prospective neural crest in Xenopus embryos, Dev. Biol. 260 (1) (2003) 79–96.
[30] S. Hauser, D. Widera, F. Qunneis, J. Müller, C. Zander, J. Greiner, C. Strauss, P. Lüningschrör, P. Heimann, H. Schwarze, J. Ebmeyer, H. Sudhoff, M.J. Araúzo-Bravo, B. Greber, H. Zaehres, H. Schöler, C. Kaltschmidt, B. Kaltschmidt, Isolation of novel multipotent neural crest-derived stem cells from adult human inferior turbinate, Stem Cells Dev. 21 (5) (2012) 742–756.
[31] T. Xu, J. Rohozinski, W. Zhao, E.C. Moorefield, A. Atala, J.J. Yoo, Inkjet-Mediated Gene Transfection into Living Cells Combined with Targeted Delivery, Tissue Eng. Part A 15 (2009) 95–101.

[32] L.D. Loozen, F. Wegman, F.C. Oner, W.J.A. Dhert, J. Alblas, Porous bioprinted constructs in BMP-2 non-viral gene therapy for bone tissue engineering, J. Mater. Chem. B 1 (2013) 6619–6626.
[33] Z. Zhua, C. Xiea, Q. Liub, X. Zhena, X. Zhenga, W. Wua, R. Lib, Y. Dingc, X. Jianga, The effect of hydrophilic chain length and iRGD on drug delivery from Poly(ε-caprolactone)-Poly(N- vinylpyrrolidone) nanoparticles, Biomaterials 32 (2011) 9525–9535.
[34] P.P. Albert, M.W. Anieke, On the density and structure formation in gels and clusters of colloidal rods and fibers, Langmuir 14 (1998) 49–54.
[35] X. Jiang, J. Li, M. Ding, H. Tan, Q. Ling, Y. Zhong, Q. Fu, Synthesis and degradation of nontoxic biodegradable waterborne polyurethanes elastomer with Poly(ε-caprolactone) and Poly(ethylene glycol) as soft segment, Eur. Polym. J. 43 (2007) 1838–1846.
[36] T. Mondal, K. Dan, J. Deb, S.S. Jana, S. Ghosh, Hydrogen- bonding-induced chain folding and vesicular assembly of an amphiphilic polyurethane, Langmuir 29 (2013) 6746–6753.
[37] E. Zaccarelli, Colloidal gels: equilibrium and non-equilibrium routes, J. Phys. Condens. Matter 19 (2007) 323101.
[38] T. Phenrat, N. Saleh, K. Sirk, R.D. Tilton, G.V. Lowry, Aggregation and sedimentation of aqueous nanoscale zerovalent iron dispersions, Environ. Sci. Technol. 41 (2007) 284–290.
[39] A.N. Hellman, K.R. Rau, H.H. Yoon, V. Venugopalan, biophysical response to pulsed laser microbeam-Induced cell lysis and molecular delivery, J. Biophotonics 1 (1) (2008) 24–35.
[40] K. Nair, M. Gandhi, S. Khalil, K.C. Yan, M. Marcolongo, K. Barbee, W. Sun, Characterization of cell viability during bioprinting processes, Biotechnol. J. 4 (2009) 1168–1177.
[41] Y. Isaka, E. Imai, Electroporation-mediated gene therapy, Expert. Opin. Drug Deliv. 4 (2007) 561–571.
[42] M. Derouazi, R. Flaction, P. Girard, M.D. Jesus, F.M. Jordan, Wurm,, Generation of recombinant Chinese hamster ovary cell lines by microinjection, Biotechnol. Lett. 28 (2006) 373–382.
[43] J. Baltich, L. Hatch-Vallier, A.M. Adams, E.M. Arruda, L.M. Larkin, Development of a scaffoldless three-dimensional engineered nerve using a nerve-fibroblast co-culture, In Vitro Cell Dev Biol Anim. 5 (2010) 438–444.
[44] K. Pfeifer, M. Vroemen, A. Blesch, N. Weidner, Adult neural progenitor cells provide a permissive guiding substrate for corticospinal axon growth following spinal cord injury, Eur J Neurosci. 20 (2004) 1695–1704.